Code Design Based on Connecting Spatially Coupled Graph Chains

Dmitri Truhachev, *Member, IEEE*, David G. M. Mitchell, *Senior Member, IEEE*, Michael Lentmaier, *Senior Member, IEEE*, Daniel J. Costello, Jr., *Fellow, IEEE*, and Alireza Karami

***Abstract*— A novel code construction based on spatially coupled low-density parity-check (SC-LDPC) codes is presented. The proposed code ensembles are comprised of several protograph-based chains characterizing individual SC-LDPC codes. We demonstrate that the code ensembles obtained by connecting appropriately chosen individual SC-LDPC code chains at specific points have improved iterative decoding thresholds. In addition, the connected chain ensembles have a smaller decoding complexity required to achieve a specific bit error probability compared to the individual code chains. Moreover, we demonstrate that, like the individual component chains, the proposed constructions have a typical minimum distance that grows linearly with block length. Finally, we show that the improved asymptotic properties of the connected chain ensembles also translate into improved finite length performance.**

***Index Terms*— Spatial graph coupling, spatially coupled codes, connected chain ensembles, protographs, LDPC convolutional codes, iterative decoding.**

I. Introduction

IT HAS been shown that the asymptotic iterative decoding performance of low-density parity-check convolutional codes (LDPC-CCs), proposed in [1], also called spatially-coupled LDPC (SC-LDPC) codes, coincides with the optimal maximum a posteriori probability (MAP) decoding performance of the underlying LDPC block codes (LDPC-BCs) [2]–[5]. The explanation for this behavior is the phenomenon of spatial graph coupling that defines the structure of SC-LDPC codes: parity-check nodes that are located at the boundaries of the graph are connected to a smaller number of variable nodes, creating stronger sub-graphs with better protected variable nodes. As iterative message-passing decoding progresses, the nodes of the stronger sub-graphs at the boundaries generate more reliable information, which propagates through the chain from iteration to iteration.

In this paper, we demonstrate that graph coupling can be extended to more general structures. In particular, we propose novel protograph-based ensembles, hereafter referred to as "connected chain ensembles", by connecting together several individual SC-LDPC code chains (referred to as "single chain ensembles"). Throughout the paper, we focus on an exemplary ensemble obtained by connecting two $(3, 6)$-regular single chains, called the "loop" ensemble, and demonstrate that the chain connection results in improved iterative decoding thresholds on the binary erasure channel (BEC) and the binary-input additive white Gaussian noise (AWGN) channel compared to individual $(3, 6)$-regular single chain ensembles of the same rate. Using a density evolution analysis, we explain the dynamics of decoding connected chain ensembles, where reliable information propagates from several directions rather than just from the ends of a single chain, thus enhancing the convergence of the overall system and reducing decoding complexity. We also provide new tools based on transfer functions to facilitate the design and analysis of connected chain ensembles.

We show that, like the component single chain ensembles, the connected chain ensembles are asymptotically good, in the sense that the minimum distance grows linearly with block length. Moreover, we consider the finite-length performance of connected chain ensembles and demonstrate via computer simulations for the AWGN channel that the error probability performance is superior to the codes obtained from single chain ensembles of the same rate and length (and thus agreeing with the finite-length scaling analysis in [6]). We note that there are several degrees of freedom in the construction of connected chain ensembles: the types of codes to be connected, the lengths of the component chains, the connection point positions, and the structure of the connections, all of which play important roles in determining the decoding characteristics and resulting performance of the connected

Manuscript received November 10, 2017; revised August 24, 2018; accepted May 4, 2019. Date of publication May 17, 2019; date of current version August 16, 2019. This work was supported in part by the National Science Foundation under Grant CCF-1161754, Grant ECCS-1710920, Grant OIA-1757207, and in part by the NSERC Canada Discovery Grant. This paper was presented in part at the 2012 Information Theory and Applications Workshop, in part at the 2012 IEEE International Conference on Communications, and in part at the 2012 IEEE International Symposium on Information Theory.

D. Truhachev and A. Karami are with the Department of Electrical and Computer Engineering, Dalhousie University, Halifax, NS B3H 4R2, Canada (e-mail: dmitry@dal.ca; akarami@dal.ca).

D. G. M. Mitchell is with the Klipsch School of Electrical and Computer Engineering, New Mexico State University, Las Cruces, NM 88011 USA (e-mail: dgmm@nmsu.edu).

M. Lentmaier is with the Department of Electrical and Information Technology, Lund University, 221 00 Lund, Sweden (e-mail: michael.lentmaier@eit.lth.se).

D. J. Costello, Jr. is with the Department of Electrical Engineering, University of Notre Dame, Notre Dame, IN 46556 USA (e-mail: costello.2@nd.edu).

Communicated by A. Jiang, Associate Editor for Coding Theory.

Color versions of one or more of the figures in this article are available online at http://ieeexplore.ieee.org.

Digital Object Identifier 10.1109/TIT.2019.2917222

chain ensembles. We conclude the paper with a short overview of possible generalizations in the design of connected chain ensembles.

Following our preliminary results [7]–[9], several research groups have investigated connecting SC-LDPC code chains to improve iterative decoding performance [10]–[12], to analyze the finite-length behavior of such constructions [6], as well as for various applications [13]–[16].

Multi-dimensional SC-LDPC codes were introduced in [10], where, instead of a sequentially coupled SC-LDPC code protograph, a two-dimensional coupled protograph was proposed. While the two-dimensional codes are more robust to bursts of erasures compared to one-dimensional single chains, they do not have a threshold advantage and suffer from higher termination rate loss. A class of multi-dimensional spatially coupled repeat-accumulate codes was later applied to coded cooperation over block-fading channels [13], demonstrating their burst error-correction capabilities. Instead of creating an entire connected two-dimensional array, a parallel interconnection of spatially coupled chains transmitted over parallel erasure channels was proposed in [14], where it was demonstrated that a chain in a better channel can help in the decoding of a chain in a degraded channel by making use of the interconnections. A modification of this construction was proposed in [11], where parallel interconnection was applied to chains of different rates to create an irregular code chain. This construction provides a flexible rate/threshold trade-off over the BEC, depending on how many chains are connected in parallel.

A code construction obtained by connecting tail-biting SC-LDPC codes was proposed recently in [12]. The graph structure of the proposed ensemble consists of two tail-biting ring graphs with joint edges at the connection point. Following a similar approach as presented in [7]–[9], the connected tail-biting ensembles are optimized for BEC thresholds, decoding complexity, and bit error rate performance. For longer chain lengths, the connected tail-biting ensembles can outperform the loop ensembles for some parameter settings, while for shorter lengths the protograph based loop ensemble is superior.

A method of continuous transmission of coupled chains, which consists of several chains connected sequentially via multiple connection points, was proposed in [15], [16], where it was shown that improved bit error rate performance compared to single-chain codes can be achieved at a cost of increased decoding complexity.

The goal of this paper is to present a general study of connected chain ensembles, giving insight into the performance improvement that can be obtained by connecting SC-LDPC code chains. In particular, this includes the methodology and guidelines for connecting chains to improve asymptotic and finite length performance, along with a toolbox for code designers to optimize designs for their desired applications.

II. Single Chain Ensembles

We start by considering a single chain SC-LDPC code ensemble. Without loss of generality, we demonstrate our approach on an ensemble of coupled $(3, 6)$-regular LDPC codes, constructed by means of protographs [17]. A protograph representing an LDPC code ensemble is a small bipartite graph connecting a set of variable nodes to a set of parity check nodes. Note that a protograph is different from the Tanner graph of a particular LDPC code, since every node of a protograph represents a set of M nodes in the Tanner graph of a particular code and every edge represents a set of M edges. The individual codes (members of the ensemble) are obtained via all possible permutations of these M edges. As such, they are represented by the same protograph. Therefore, a protograph with a *lifting factor* of M describes an ensemble of LDPC codes. It is an important feature of this construction that each lifted code inherits the degree distribution and graph neighborhood structure of the protograph.

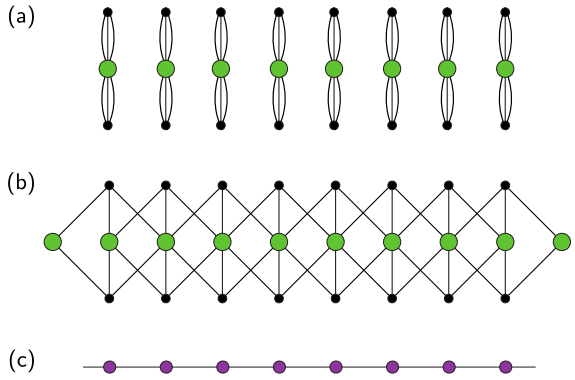

Fig. 1. Tanner graphs associated with (a) a chain of L uncoupled $(3, 6)$-regular LDPC-BC protographs for $L = 8$ and (b) a single chain of L spatially coupled $(3, 6)$-regular LDPC-BC protographs for $L = 8$. The larger circles in the figure correspond to parity-check nodes and the smaller solid circles correspond to variable nodes. Also shown in (c) is a simplified illustration of the $(3, 6)$-regular single chain protograph of length $L = 8$. Each node illustrates a segment consisting of one check node and two variable nodes.

A single chain SC-LDPC ensemble can be constructed by *coupling* together several LDPC-BC ensembles by "spreading" edges from variables nodes of each copy to neighboring check nodes, forming a chain (see, *e.g.*, [18]). Fig. 1 shows representative Tanner graphs for (a) a group of $L = 8$ uncoupled $(3, 6)$-regular LDPC-BC ensemble protographs, (b) a single chain SC-LDPC ensemble protograph, and (c) a simplified illustration of the single chain protograph where each segment is illustrated by a single node. Note that, by coupling the block code protographs in this way, we introduce a "structured irregularity" into the coupled protograph. In this example all of the variable nodes still have 3 edge connections; however, the check nodes at the start and the end of the chain are only connected to either 2 or 4 variable nodes. For this $(3, 6)$-regular single chain SC-LDPC code ensemble, we find that the *threshold saturation* effect improves the belief propagation (BP) threshold (for a BEC with erasure probability ϵ) from the uncoupled BP threshold $\epsilon_{\text{BP}} = 0.4294$ to a value numerically indistinguishable from the (optimal) MAP threshold $\epsilon_{\text{MAP}} = 0.4881$ as the coupling length L becomes sufficiently large [2], [3].

The associated incidence matrix $\mathbf{B}$ of the protograph is called the *base* matrix. The parity-check matrix $\mathbf{H}$ of a protograph-based LDPC-BC can be created by replacing each

TABLE I

BEC THRESHOLDS ϵ^* FOR SEVERAL LOOP ENSEMBLES $\bar{\mathcal{L}}(3, 6, L)$ WITH CONNECTION PLACEMENT OPTIMIZED FOR BEC THRESHOLD MAXIMIZATION ALONGSIDE THE THRESHOLDS OF THE CORRESPONDING LOOP ENSEMBLES $\mathcal{L}(3, 6, L)$ AND SINGLE CHAIN ENSEMBLES $\mathcal{C}(3, 6, L)$

Rate	Ensemble	ϵ^*	L'	Ensemble	ϵ^*	L'	Ensemble	ϵ^*
0.3750	$\bar{\mathcal{L}}(3,6,8)$	0.5509	2	$\mathcal{L}(3,6,8)$	0.5509	2	$\mathcal{C}(3,6,8)$	0.5223
0.3889	$\bar{\mathcal{L}}(3,6,9)$	0.5424	2	$\mathcal{L}(3,6,9)$	0.5382	3	$\mathcal{C}(3,6,9)$	0.5120
0.4167	$\bar{\mathcal{L}}(3,6,12)$	0.5238	4	$\mathcal{L}(3,6,12)$	0.5238	4	$\mathcal{C}(3,6,12)$	0.4954
0.4286	$\bar{\mathcal{L}}(3,6,14)$	0.5125	5	$\mathcal{L}(3,6,14)$	0.5106	4	$\mathcal{C}(3,6,14)$	0.4910
0.4333	$\bar{\mathcal{L}}(3,6,15)$	0.5105	5	$\mathcal{L}(3,6,15)$	0.5105	5	$\mathcal{C}(3,6,15)$	0.4899
0.4412	$\bar{\mathcal{L}}(3,6,17)$	0.5034	6	$\mathcal{L}(3,6,17)$	0.4989	5	$\mathcal{C}(3,6,17)$	0.4887
0.4444	$\bar{\mathcal{L}}(3,6,18)$	0.4989	6	$\mathcal{L}(3,6,18)$	0.4989	6	$\mathcal{C}(3,6,18)$	0.4884
0.4474	$\bar{\mathcal{L}}(3,6,19)$	0.4980	7	$\mathcal{L}(3,6,19)$	0.4953	6	$\mathcal{C}(3,6,19)$	0.4883
0.4500	$\bar{\mathcal{L}}(3,6,20)$	0.4953	7	$\mathcal{L}(3,6,20)$	0.4927	6	$\mathcal{C}(3,6,20)$	0.4882

non-zero entry $B_{i,j}$ in $\mathbf{B}$ by a sum of $B_{i,j}$ non-overlapping permutation matrices of size M and each zero entry by the $M \times M$ all-zero matrix. In graphical terms, this can be viewed as taking an M-fold graph cover or "lifting" of the protograph. We denote the $(3, 6)$-regular single chain ensemble protograph of length L by $\mathcal{C}(3, 6, L)$. The design rate of the ensemble $\mathcal{C}(3, 6, L)$ is given by[1]

$$R(\mathcal{C}(3, 6, L)) = \frac{L-2}{2L}, \tag{1}$$

which increases monotonically with L and approaches $1/2$ as $L \to \infty$.

III. CONNECTED CHAIN ENSEMBLES

In this section, we present a thorough overview of connected chain ensembles. Beginning with motivation in Section III-A, we then proceed by presenting an example of a connected ensemble, which we call *the loop ensemble*, in Section III-B. We first focus on the BEC and demonstrate that the loop ensemble has a better threshold compared to single chains of the same rate. We then follow a density evolution analysis to demonstrate the empirical reasons for threshold improvement in Section III-C and study general properties of chain interconnection in Section III-D. We then also demonstrate improvements in terms of decoding complexity, threshold, and finite length performance on AWGN channel, and we show that the constructed ensembles are asymptotically good in terms of minimum distance in Sections III-E, III-F, and III-G, respectively.

A. Motivation

While it is customary to focus on threshold saturation for long single chain ensembles and emphasize the role of the coupling effect in their threshold improvement, shorter single chains are important objects by themselves. As the length L of the chain increases, starting from $L = 3$, we observe a spectrum of single chain ensembles $\mathcal{C}(3, 6, L)$ that demonstrate a trade-off between rate and threshold (see Tables I and II). In particular, we notice that for short chains the threshold for the BEC may exceed 0.5, which, of course, comes at the price of rate loss (1). In addition to improved thresholds, spatially coupled ensembles reduce the decoding complexity (in terms of the number of operations performed per variable node) required to achieve a desired decoding error probability.

[1]Here R denotes the design rate of the ensembles. The actual rate of a particular member of the ensemble may be slightly higher due to possible linear dependencies between the rows in its parity-check matrix.

TABLE II

AWGN CHANNEL THRESHOLDS IN TERMS OF σ^* CALCULATED FOR THE $\mathcal{L}(3, 6, L)$ LOOP ENSEMBLES AND THE $\mathcal{C}(3, 6, L)$ SINGLE CHAIN ENSEMBLES FOR $L = 8$, 12, 15, AND 18

Rate	Ensemble	σ^*	Ensemble	σ^*
0.3750	$\mathcal{L}(3,6,8)$	1.0566	$\mathcal{C}(3,6,8)$	1.0079
0.4167	$\mathcal{L}(3,6,12)$	1.0160	$\mathcal{C}(3,6,12)$	0.9632
0.4333	$\mathcal{L}(3,6,15)$	0.9878	$\mathcal{C}(3,6,15)$	0.9526
0.4444	$\mathcal{L}(3,6,18)$	0.9690	$\mathcal{C}(3,6,18)$	0.9490

Given these interesting properties and trade-offs of single chain ensembles, we now consider new connected chain ensembles for which single chains serve as building blocks. We can set several goals or targets for such a construction. The most obvious targets, which we focus on in this paper, include improved rate/threshold trade-offs, faster convergence to the limiting performance, and smaller decoding complexity. Other targets could be, e. g., improved finite length performance and unequal error protection [15]. Single chain ensembles of the same rate can serve as reference points for performance comparison.

One way to explain the basic intuition behind the benefits of connecting chains is as follows. Throughout the decoding process on a single chain, the reliable information spreads from the graph boundaries to the middle part of the chain. In a connected chain ensemble the connection points create other strong sub-codes, enabling reliable information to propagate from other parts of the graph, thereby improving decoding convergence. In addition, longer chains are effectively broken into shorter segments with better thresholds (see Section III-D).

B. Example: The Loop Ensemble

Consider two single chain protographs of length L connected by edges as shown in Fig. 2 (a). The last segment of the upper chain is connected to an inner segment of the lower chain, while the first segment of the lower chain is connected

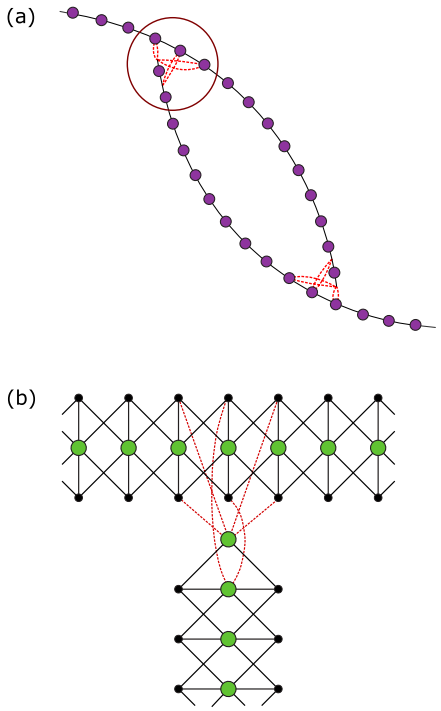

Fig. 2. (a) Two single chain protographs of length $L = 15$ connected as a loop. (b) Connection point in detail.

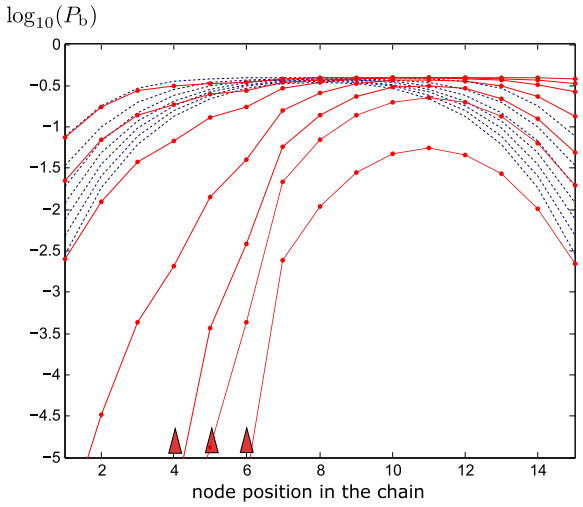

Fig. 3. Logarithm of the average bit erasure probability for the variable nodes of the upper chain for the ensembles $\mathcal{L}(3, 6, 15)$ (solid curves) and $\mathcal{C}(3, 6, 15)$ (dashed curves), as a function of the position of the node in the chain. The curves (either solid or dashed) are computed for decoding iterations $1, 6, 11, \ldots, 31$ (from top to bottom). The three positions where the upper chain is connected to the end of the lower chain in the loop are shown by the triangles.

to an inner segment of the upper chain. The connections between the end of one chain and the inner part of the other chain are made as depicted in Fig. 2 (b). (Justification for this design and variations on the construction will be given later.) Recall that a parity check node located at the beginning of a $(3, 6)$-regular SC-LDPC protograph chain has only two outgoing edges, while the parity check node next to it has only four outgoing edges (instead of 6). Focusing on the circled connection in Fig. 2 (a), four extra edges are added to the first check node of the lower chain and connected to variable nodes in the upper chain. Similarly, two extra edges are added to the second check node of the lower chain and connected to variable nodes in the upper chain. The connection point between the last segment of the upper chain and the inner part of the lower chain is made in the same way.

The connection points are located at a distance of $\lfloor L/3 \rfloor$ from the chain boundaries. We denote the loop ensemble consisting of two $(3, 6)$-regular single chains of length L by $\mathcal{L}(3, 6, L)$. Since the loop is constructed from two equal length chains, the rate of this ensemble is equal to the rate of a single chain, *i.e.*,

$$R(\mathcal{L}(3, 6, L)) = R(\mathcal{C}(3, 6, L)) = \frac{L-2}{2L}. \tag{2}$$

C. Density Evolution and Iterative Decoding Convergence

Consider communication over a BEC with erasure probability ϵ using the $\mathcal{L}(3, 6, 15)$ loop ensemble and the $\mathcal{C}(3, 6, 15)$ single chain ensemble. We utilize density evolution to compute bit erasure probabilities at each node of the protograph for every decoding iteration. Using this tool we relate the evolution of the erasure probability to the node position in the protograph and compare the erasure probability behavior of the loop and single chain ensembles.

We denote the set of variable protograph nodes connected to check node k by $\mathbb{V}(k)$ and the set of check protograph nodes connected to variable node j by $\mathbb{C}(j)$. The probability that the message passed from check node k to variable node j at iteration i is an erasure is denoted by $q_{kj}^{(i)}$. The probability of an erasure message from variable node j to check node k is similarly denoted by $p_{jk}^{(i)}$. The following equations relate the erasure probabilities of the messages at different iterations:

$$q_{kj}^{(i)} = 1 - \prod_{j' \in \mathbb{V}(k) \setminus j} (1 - p_{j'k}^{(i-1)}) \tag{3}$$

$$p_{jk}^{(i)} = \epsilon \prod_{k' \in \mathbb{C}(j) \setminus k} q_{k'j}^{(i)}. \tag{4}$$

The variable node messages are initialized as $p_{jk}^{(0)} = \epsilon$ at iteration 0. The bit erasure probability of the variable nodes at iteration i can be calculated as

$$P_b(j) = \epsilon \prod_{k \in \mathbb{C}(j)} q_{kj}^{(i)}. \tag{5}$$

The evolution of the bit erasure probability for the variable nodes of the $\mathcal{L}(3, 6, 15)$ ensemble is illustrated in Fig. 3. The solid curves with circle markers correspond to the erasure probability at each node position in the upper chain of the loop at iterations $1, 6, 11, \ldots, 31$ (from top to bottom).[2] The dashed curves correspond to the erasure probability as a function of the node position for the single chain ensemble $\mathcal{C}(3, 6, 15)$ and iteration numbers $1, 6, 11, \ldots, 31$. The BEC erasure probability is fixed to be $\epsilon = 0.488$. We notice that the solid curves display lower error probability values with fewer

[2]Due to the symmetric nature of the loop construction, it is sufficient to consider the evolution of the bit erasure probability for only one chain.

iterations than the dashed curves, and hence it takes fewer decoding iterations for the ensemble $\mathcal{L}(3, 6, 15)$ to converge to a given bit erasure probability value.

Note that each dashed curve displays a symmetric concave-shape; however, the shape of the solid curves is not symmetric. This is due to the fact that the loop protograph is comprised of two connected chains. The inner part of the upper chain is connected to the lower chain by edges connecting to its nodes at positions 4, 5, and 6, shown by triangles on the figure. Note that the solid curves dip down at these positions since the lower chain provides convergence improvement via the connection. The connection point creates a stronger sub-graph in which the variable nodes are connected to four check nodes instead of three. This sub-graph distributes more reliable information to its neighborhood (similar to the "open end," positions 1 and 2, of the upper chain) throughout the decoding process.

On the other hand, the rightmost open end of the upper chain (positions 14 and 15) converges to low bit erasure probability values more slowly than for the single chain. This can be observed by comparing the solid curves to the corresponding dashed curves. The reason for this behavior is the additional connecting edges present at the end of the upper chain that are now used to connect it to the lower chain, thereby increasing the check node degrees. These edges are absent in the single chain case. However, convergence at the end of the upper chain improves with subsequent iterations as the lower chain starts to converge, due to the increased connectivity of its variable nodes. Eventually, the lower solid curve displays a concave shape as a result of the more reliable information coming from the lower chain.

To summarize, the two connected chains create a balanced system in which one helps the other to converge and vice versa. The distances between the connection points as well as the positions of the edges connecting the two chains are important parameters. Those parameters, employed in the Fig. 2 example, were optimized in [8]. The results of the optimization are intuitively satisfying: the connection points should be sufficiently strong to enable the open ends and the connection points to be robust, breaking the chains into equal-size pieces that converge simultaneously (see [7], [8] for details, as well as Section III-D for tools to analyze and design such balanced systems).

The improved convergence behavior resulting from the balanced exchange of reliable information between the two chains implies more robustness to channel noise. One of the consequences is seen in improved iterative decoding thresholds of the connected chain ensembles. We recall that the BEC iterative decoding threshold is the supremum of the values of the erasure probability ϵ for which codes from the ensemble can be decoded reliably (for sufficiently large lifting factor M) [19], [20].

The BEC thresholds ϵ^* for loop ensembles with several values of L between 8 and 20 are shown in Table I. The first column shows the rate of the ensembles. The next three columns list threshold values for the loop ensembles $\bar{\mathcal{L}}(3, 6, L)$ where the connection point position L' (the distance between the connection point and the chain boundary) has been optimized using Proposition 2 from Section III-D in order to maximize the BEC threshold. The next three columns present values for the regular loop ensembles $\mathcal{L}(3, 6, L)$ with $L' = \lfloor L/3 \rfloor$. The last two columns give the values for the single chain ensembles of the same rate. It is observed that the thresholds of the connected ensembles are always better than the thresholds of the corresponding single chain ensembles. Connecting the chains at a distance $L' = \lfloor L/3 \rfloor$ from the chain boundaries results in the highest threshold in most cases, however, for some lengths, such as $L = 14, 17, 19, 20$ connecting at distance $L' = \lceil L/3 \rceil$ gives better results, while for $L = 9$ the best connection is at distance $L' = 2$.

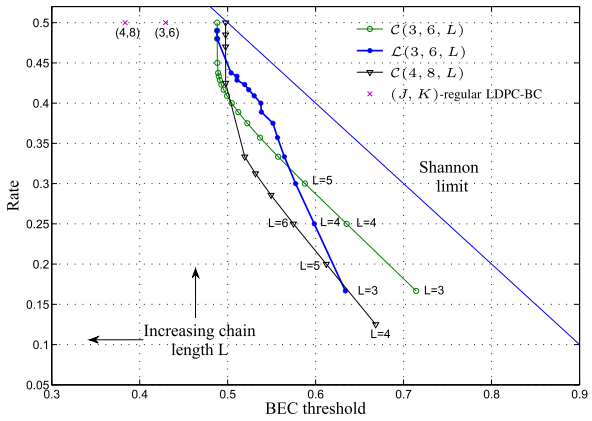

Fig. 4. BEC thresholds for the $\mathcal{L}(3, 6, L)$ loop ensembles as well as some $\mathcal{C}(J, K, L)$ ensembles and (J, K)-regular LDPC-BC ensembles.

AWGN channel thresholds for the loop ensembles $\mathcal{L}(3, 6, L)$ are given in Table II for $L = 8, 12, 15$, and 18, and the results for the corresponding single chain ensembles $\mathcal{C}(3, 6, L)$ are shown for comparison. These AWGN channel thresholds (given in terms of the standard deviation σ^* of the noise) are computed using discretized density evolution [21]. This method is more complex than the Gaussian approximation, but it gives exact results for a quantized AWGN channel model and hence provides a strict bound on the thresholds of the continuous AWGN channel. The trade-off between complexity and accuracy can be controlled by the number of quantization intervals and the supported range. The presented results correspond to 8 bit quantization of the log-likelihood ratios within the interval $[-20, 20]$. Again, we notice that the thresholds of the loop ensembles are significantly better than for the corresponding single chains.

Fig. 4 shows the BEC thresholds for the $\mathcal{L}(3, 6, L)$ ensembles in comparison to the $\mathcal{C}(3, 6, L)$ and $\mathcal{C}(4, 8, L)$ single chain ensembles for a variety of chain lengths L. Comparing the $\mathcal{L}(3, 6, L)$ ensembles to the $\mathcal{C}(3, 6, L)$ ensembles, we observe that, for $L > 5$, the thresholds of the loop ensembles are generally superior although the thresholds converge as L increases.[3]. In particular, we observe a dramatic threshold improvement for the loop ensembles with rates in the region $0.33 \leq R \leq 0.47$. The thresholds of the single chain ensembles $\mathcal{C}(3, 6, L)$ and $\mathcal{C}(4, 8, L)$ are observed to converge

[3]Again, this is intuitive since the two connection points have diminishing contributions as the chains grow longer. Convolutional constructions with a linearly growing number of connection points can maintain the advantage, however (see [15]).

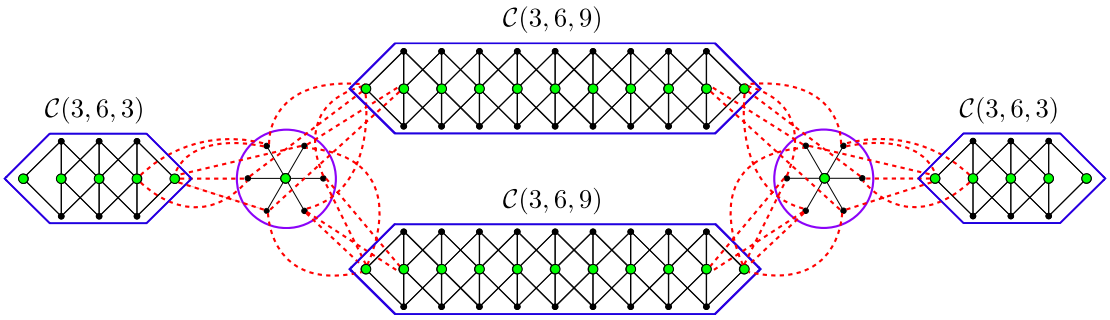

Fig. 5. The loop $\mathcal{L}(3,6,15)$ consisting of two $\mathcal{C}(3,6,3)$ sub-chains, two $\mathcal{C}(3,6,9)$ sub-chains, and two connection points.

TABLE III
BEC THRESHOLDS ϵ^* FOR SEVERAL LOOP ENSEMBLES $\mathcal{L}(3,6,L)$, UPPER AND APPROXIMATE LOWER BOUNDS

Rate	Ensemble	ϵ^*	Upper bound (Proposition 1)	Threshold approximation (Proposition 2)
0.3750	$\mathcal{L}(3,6,8)$	0.5509	0.5878	0.5513
0.4167	$\mathcal{L}(3,6,12)$	0.5238	0.5367	0.5244
0.4333	$\mathcal{L}(3,6,15)$	0.5105	0.5120	0.5103
0.4444	$\mathcal{L}(3,6,18)$	0.4989	0.4992	0.4989

to values close to the MAP thresholds of the underlying $(3,6)$- and $(4,8)$-regular LDPC-BC ensembles as L becomes sufficiently large. As a result, for large L, we observe that the iterative decoding thresholds of the $\mathcal{C}(4,8,L)$ ensembles are larger than those of the $\mathcal{C}(3,6,L)$ ensembles (unlike the corresponding LDPC-BC ensembles). However, even in this region, *i.e.*, for rates between 0.40 and 0.45, we observe that the thresholds of the $\mathcal{L}(3,6,L)$ ensemble remain above the $\mathcal{C}(4,8,L)$ thresholds. In general, using stronger components can create stronger connected chain ensembles, *i.e.*, loops constructed using $(4,8)$-regular single chain protographs can achieve further performance improvement over those using $(3,6)$-regular single chains (see Section IV).

D. The Principles of Chain Interconnection

The overall connected ensemble protograph can be viewed as comprised of a number of single chain protographs (sub-chains) along with some simple protographs corresponding to the connection points. In order to study the iterative decoding performance of connected chain ensembles in more detail and provide tools for their design, we now focus on the interaction between the sub-chains and the connection point protographs that comprise the overall protograph of the connected system throughout the decoding process. The analysis principles we present apply to a large variety of connected chain ensembles, including connected regular $\mathcal{C}(J,K,L)$ chains and ARJA and AR4JA chains (see Section IV). Here we illustrate the approach using the $\mathcal{L}(3,6,15)$ ensemble as an example.

A graphical representation of the loop ensemble $\mathcal{L}(3,6,15)$ and the six parts (sub-graphs) forming its protograph is given in Fig. 5. The overall protograph consists of two $\mathcal{C}(3,6,3)$ sub-chain protographs connected on only one side, two $\mathcal{C}(3,6,9)$ sub-chain protographs connected on both sides, and two connection point protographs, each consisting of one check node of degree six and six variable nodes of degree four.

The edges exchanging information between the connected sub-graphs are shown by dashed lines in Fig. 5. Note that the dashed edges connect check nodes of the sub-chains to variable nodes of the connection points. Throughout the decoding process those edges carry messages of a certain reliability. In order to produce an upper bound on the threshold of the connected chain ensemble, we can assume that the messages passed along the dashed connection edges are completely reliable. This assumption is equivalent to disconnecting all the sub-chains forming the connected chain ensemble and decoding them separately. This observation leads us to the following statement.

Proposition 1. *The threshold of the connected chain ensemble is upper bounded by the minimum of the thresholds of all its sub-chains.*

For the case of the loop ensemble, the threshold of $\mathcal{L}(3,6,15)$ for the BEC equals 0.5105 and is upper bounded by the minimum of the thresholds of $\mathcal{C}(3,6,3)$ and $\mathcal{C}(3,6,9)$, which equals 0.512. Table III shows respective BEC threshold upper bounds for loop ensembles of lengths 12, 15, and 18.

For the purpose of threshold analysis we consider the following *decoding schedule* which runs on both global iteration and local iteration clocks. We call it a *global-local* schedule. In the first phase of each global iteration, all sub-chains perform decoding until the probabilities of erasure at all their nodes become fixed, *i.e.*, a fixed point (or steady state) is reached. This may require a different number of decoding iterations for each sub-chain. In the second phase of each global iteration connection points perform their variable-check-variable node operations on the messages incoming

from the connected sub-chains and return a new set of messages to the sub-chains. Note that the overall thresholds of connected systems for the conventional alternating check-variable node decoding schedule and for the global-local schedule coincide, although the global-local schedule may require more iterations to converge. We consider it here, however, because it simplifies the threshold analysis.

We now define several functions describing the change of the erasure probability at the connecting edges for one global iteration and use them to estimate the threshold of the overall connected chain ensemble. Consider as an example a protograph of the single chain ensemble $\mathcal{C}(3, 6, L)$ of length L and assume that it has six additional edges outgoing from the two check nodes located at the left end of the protograph chain and six additional edges outgoing from the two check nodes located at the right end of the protograph chain. Either of the two sub-chains of length 9 depicted in Fig. 5 with six connecting edges on each end illustrates the case of $L = 9$. Assume that each of the six additional edges on the left end of the chain carries a message with erasure probability $p_{\text{in,left}}$ and each of the six additional edges on the right carries a message with erasure probability $p_{\text{in,right}}$.

Assuming a channel erasure probability of ϵ, we perform iterative decoding on the chain for a number of iterations until all its nodes reach steady-state. After that we measure the erasure probability on the additional edges on the left side of the chain and define a function $f^{(L)}_{\text{out,left}}(p_{\text{in,left}}, p_{\text{in,right}}, \epsilon)$ that equals the *average* erasure probability among the additional edges on the left. Similarly we define a function $f^{(L)}_{\text{out,right}}(p_{\text{in,left}}, p_{\text{in,right}}, \epsilon)$ that gives the average erasure probability on the right. We call the functions $f^{(L)}_{\text{out,left}}(\cdot)$ and $f^{(L)}_{\text{out,right}}(\cdot)$ *input/output transfer functions*.

We also now define an input/output transfer function for the connection point. When all probabilities on the incoming edges to the connection point are the same and equal to p_{in}, it is given by

$$g_{\text{out}}(p_{\text{in}}, \epsilon) = \epsilon p_{\text{in}}^2 \left[1 - (1 - \epsilon p_{\text{in}}^3)^5\right]$$

for the $(3, 6)$-regular LDPC connection point depicted in Fig. 5. More generally, for (J, K)-regular LDPC connection points where all the variable node degrees equal $J + 1$, it is given by

$$g_{\text{out}}(p_{\text{in}}, \epsilon) = \epsilon p_{\text{in}}^{J-1} \left[1 - (1 - \epsilon p_{\text{in}}^{J})^{K-1}\right].$$

Fig. 6 demonstrates three bundles of transfer functions corresponding to $f^{(3)}_{\text{out,right}}(0, p_{\text{in}}, \epsilon)$, $f^{(9)}_{\text{out,left}}(p_{\text{in}}, p_{\text{in}}, \epsilon)$, and $g^{-1}_{\text{out}}(p_{\text{in}}, \epsilon)$ for $\epsilon = 0.49, 0.5, 0.51, 0.52$. The function $f^{(3)}_{\text{out,right}}(0, p_{\text{in}}, \epsilon)$ represents the behavior of the $\mathcal{C}(3, 6, 3)$ ensemble, which has no connections at its left end and is connected to the connection point at its right end within the loop ensemble (see Fig. 5). Hence the first argument of the function is set to 0 while the second argument is set to p_{in}. The function $f^{(9)}_{\text{out,left}}(p_{\text{in}}, p_{\text{in}}, \epsilon)$ represents the behavior of the $\mathcal{C}(3, 6, 9)$ ensemble, which has connection points at both its left and right ends. Due to the symmetry of the loop protograph

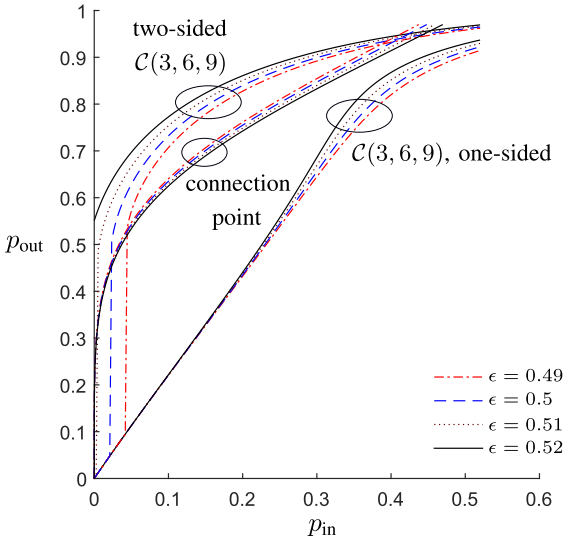

Fig. 6. Three bundles of transfer functions from right to left: a $\mathcal{C}(3, 6, 3)$ chain connected from one side, a connection point, a $\mathcal{C}(3, 6, 9)$ connected from two sides. The solid, dotted, dashed, and dash-dotted curves correspond to $\epsilon = 0.52, 0.51, 0.50, 0.49$, respectively.

around the two connection points (see Fig. 5), we set the first two arguments of the function to p_{in}.

The function $f^{(3)}_{\text{out,right}}(0, p_{\text{in}}, \epsilon)$ is (almost) linear for small p_{in}, but changes shape for larger p_{in}. This behavior is due to the fact that, for small p_{in}, when the operating channel erasure probability ϵ is below the threshold of the single chain ensemble $\mathcal{C}(3, 6, 3)$, the open-ended chain converges and therefore the output is dominated by a function of the input probability p_{in} (which is kept constant). In turn, for small p_{in} the output function is dominated by its linear terms. The situation is similar for $f^{(9)}_{\text{out,left}}(p_{\text{in}}, p_{\text{in}}, \epsilon)$ in the case of small p_{in}, e.g., $\epsilon = 0.49, 0.5$, and 0.51, which are all below the convergence threshold 0.512 of $\mathcal{C}(3, 6, 9)$. However, as p_{in} grows, there is a sharp transition to another regime in which the input probability is too large for the chain to converge, even below its threshold. For the case of $\epsilon = 0.52$, the chain does not converge, even for $p_{\text{in}} = 0$, and therefore the linear behavior is not present.

Now consider once again the connected system representation given in Fig 5. Due to symmetry, we can focus on one connection point which connects two $\mathcal{C}(3, 6, 9)$ sub-chains and one $\mathcal{C}(3, 6, 3)$ sub-chain. In order to determine the loop threshold, we match the input/output transfer function of the connection point to the average input/output transfer function of the sub-chains. Note that, by averaging the input and output probabilities over the six edges connecting each sub-chain to the connection point, the computed threshold values are approximate. They are nevertheless close to the true threshold values (see Table III). We now formulate the developed analysis approach as a Proposition for the general case of $\mathcal{L}(3, 6, L)$ loop with connection points located at distance L' from the chain boundaries.

Proposition 2. *The threshold of the loop ensemble is approximately equal to the maximum channel erasure probability* ϵ

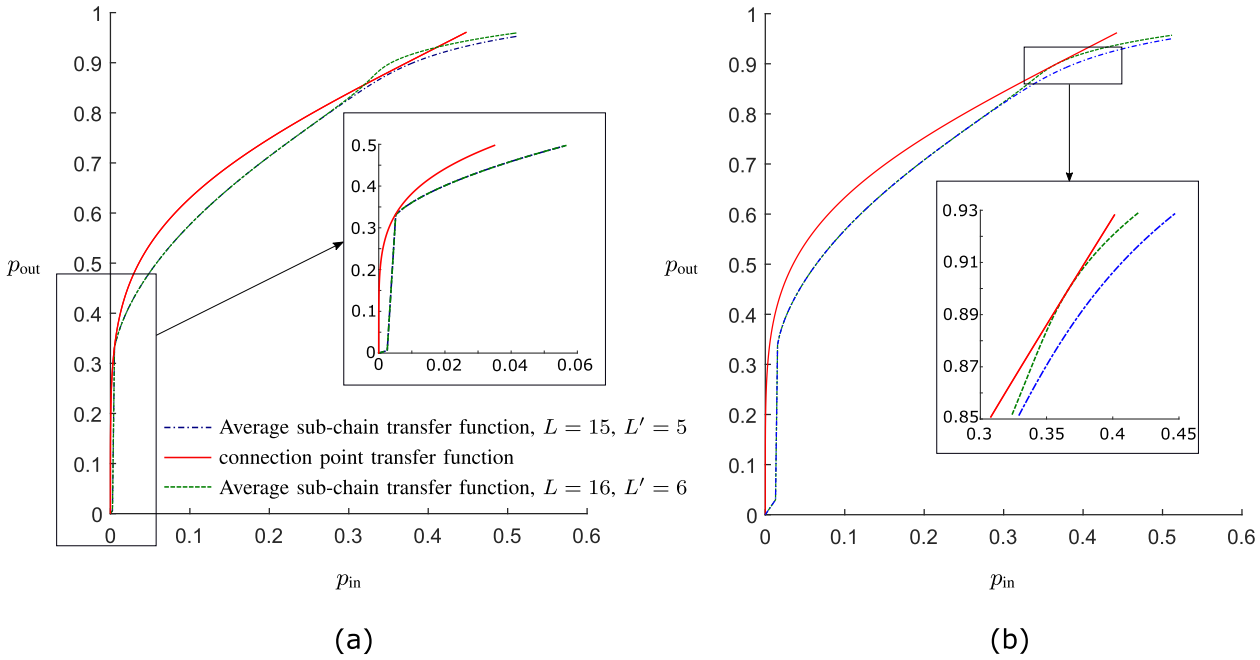

Fig. 7. The input/output transfer function chart for the case of (a) $\epsilon = 0.5103$ and (b) $\epsilon = 0.5040$. By p_{in} we denote the average input probability to the connection point and by p_{out} the average output probability.

such that the only non-negative fixed point of the equation

$$p = g_{\text{out}}\left(\frac{1}{3}\left(f_{\text{out,right}}^{(L'-1)}(0, p, \epsilon) + 2 f_{\text{out,left}}^{(L-L'-2)}(p, p, \epsilon)\right), \epsilon\right), \quad (6)$$

or equivalently

$$g_{\text{out}}^{-1}(p) = \frac{1}{3}\left(f_{\text{out,right}}^{(L'-1)}(0, p, \epsilon) + 2 f_{\text{out,left}}^{(L-L'-2)}(p, p, \epsilon), \epsilon\right), \quad (7)$$

is $p = 0$, where L' is the distance from the connection point to the chain boundaries.

Fig. 7 demonstrates an input/output transfer function chart corresponding to Proposition 2 for the case of (a) $\epsilon = 0.5103$ and (b) $\epsilon = 0.5040$. The dash-dotted curves correspond to the average connection point input for the case of the loop ensemble $\mathcal{L}(3, 6, 15)$ (see the right hand side of (7)). The dashed curves correspond to the average connection point input for the case of a slightly modified loop ensemble with the same inner chains $\mathcal{C}(3, 6, 9)$ but longer outer chains $\mathcal{C}(3, 6, 4)$. The latter case corresponds to $L = 16$, i.e. $\mathcal{L}(3, 6, 16)$ loop, and $L' = 6$.

The connection point transfer function is shown as the solid curve. We note that the transfer chart provides a good indication of the system's convergence threshold, which is the BEC probability ϵ for which the convergence tunnel between the curves closes up. We also note that, for the example illustrated in Fig. 7, the longer outer chain results in a lower threshold for the overall connected system. Table III gives the estimated thresholds obtained using input/output transfer function charts and compares them to the upper bounds obtained using Proposition 1 for the case of loop ensembles $\mathcal{L}(3, 6, 8)$, $\mathcal{L}(3, 6, 12)$, $\mathcal{L}(3, 6, 15)$ and $\mathcal{L}(3, 6, 18)$.

We can now use Proposition 2 to find the optimal connection point location L' for loop ensembles. Fig. 8 demonstrates the threshold values of the $\mathcal{L}(3, 6, L)$, $L = 6, 7, \cdots, 21$, (regular) loop ensembles with $L' = \lfloor L/3 \rfloor$ (solid curve with circles) and the loop ensembles $\bar{\mathcal{L}}(3, 6, L)$ with optimized connection point placement L' listed in Table I, Section III-C, obtained by maximizing the predicted threshold value of Proposition 2 (dash-dotted curve with circles). The upper bounds on the threshold values obtained using Proposition 1 are given by the solid curve with stars for $\mathcal{L}(3, 6, L)$ and the dash-dotted curve with stars for $\bar{\mathcal{L}}(3, 6, L)$. The predicted thresholds given by Proposition 2 are plotted by the solid curve with squares for $\mathcal{L}(3, 6, L)$ and the dash-dotted curve with squares for $\bar{\mathcal{L}}(3, 6, L)$. We note that the approximation is very close for all values of L, while the upper bound provides a good threshold approximation for larger values of L as well.

Based on this example, we see that input/output transfer function charts provide a useful tool for designing connected chain ensembles. One can use the input/output transfer function charts of the system components (sub-chains and connection points) to visually estimate the critical channel parameter ϵ for which the decoding erasure probability reaches a zero steady-state value for each part of the connected system.

E. Decoding Complexity

To compare the decoding complexity of connected and single chain ensembles, we consider transmission over the BEC and simultaneous decoding of the entire code graph, where we employ the node updating schedule proposed in [22]. The algorithm designates a target bit erasure probability $P_{\text{b,max}}$ as well as an update improvement parameter θ. Regular message

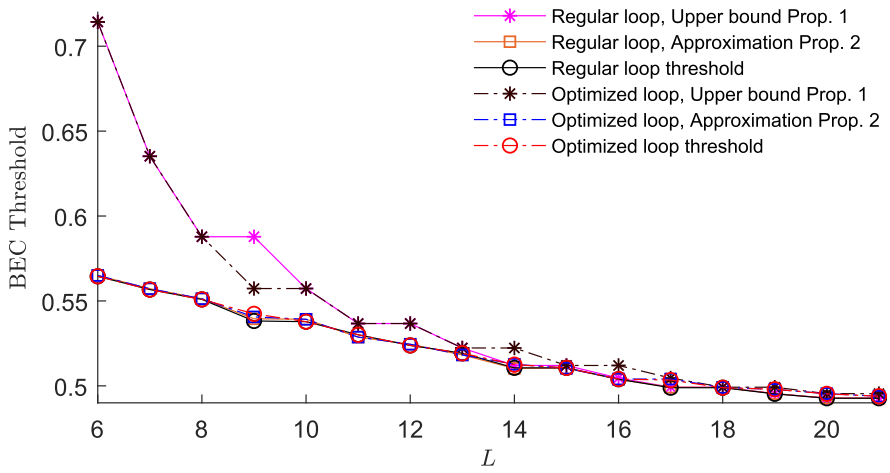

Fig. 8. Threshold values for the loop $\mathcal{L}(3, 6, L)$ ensembles (solid curve with circles) and optimized loop $\bar{\mathcal{L}}(3, 6, L)$ ensembles (dash-dotted curve with circles) on the BEC compared to the upper bound given by Proposition 1 (solid and dash-dotted curves with stars) and the approximation of Proposition 2 (solid and dash-dotted curves with squares).

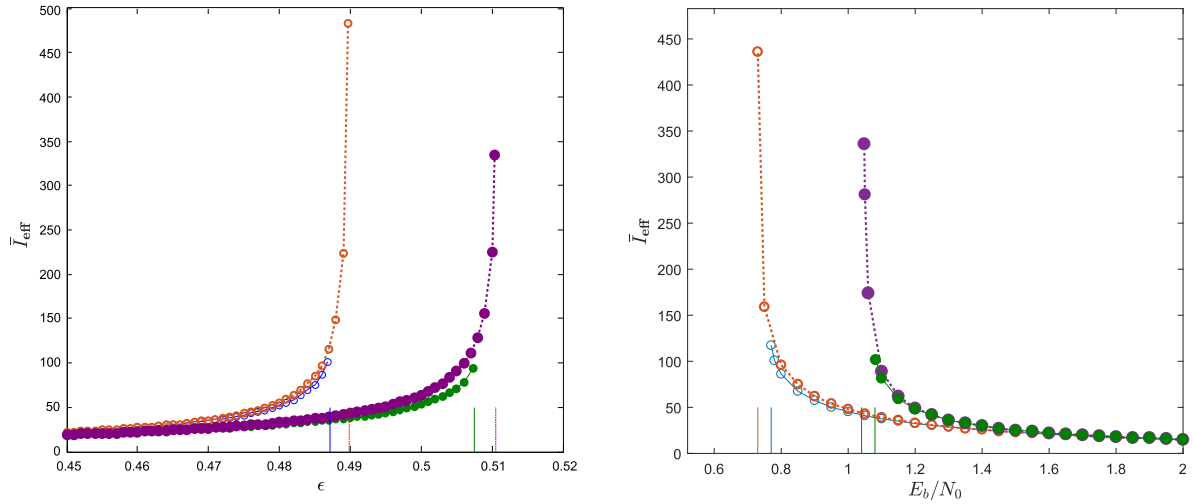

Fig. 9. The average number of updates per node $\bar{I}_{\text{eff}}$ as a function of the BEC erasure probability ϵ (left) and the AWGN channel signal-to-noise ratio E_{b}/N_0 (right) for the $\mathcal{L}(3, 6, 15)$ ensemble (curves with solid circles) and the $\mathcal{C}(3, 6, 15)$ ensemble (curves with hollow circles). The dashed curves are computed for the updating schedule with improvement parameter $\theta = 0$, while the solid curves are for $\theta = 10^{-2}$. The corresponding thresholds are given by vertical lines.

passing updates are performed for each variable or check node with the following exceptions:

- no update for variable node j is performed if the bit erasure probability $P_{\text{b}}(j) < P_{\text{b,max}}$;
- no update for any variable node j or any check node k is performed if all the nodes in $\mathbb{C}(j)$ or $\mathbb{V}(k)$, respectively, were not updated in the previous iteration;
- no update for variable node j is performed if the potential improvement of the bit erasure probability is less than θ, *i.e.*, if

$$\frac{P_{\text{b,old}}(j) - P_{\text{b,new}}(j)}{P_{\text{b,old}}(j)} < \theta. \tag{8}$$

We set the target bit erasure probability $P_{\text{b,max}}$ to 10^{-5} and the resulting number of updates per node $\bar{I}_{\text{eff}}$ (for both check and variable nodes), averaged over the node positions, is considered as a measure of decoding complexity.

The *average number of updates per node* $\bar{I}_{\text{eff}}$ is plotted in Fig. 9 (left) as a function of the BEC erasure probability ϵ for the single chain ensemble $\mathcal{C}(3, 6, 15)$ (hollow circles) and the loop ensemble $\mathcal{L}(3, 6, 15)$ (solid circles). The dashed curves correspond to the updating schedule with the improvement parameter $\theta = 0$ (in which case the nodes are always updated), while the solid curves correspond to $\theta = 10^{-2}$. The vertical straight lines indicate the iterative decoding thresholds calculated for each construction with the corresponding update schedule. We observe a significant complexity improvement provided by the connected chain construction.

For transmission over the AWGN channel, $\bar{I}_{\text{eff}}$ is plotted as a function of the signal-to-noise ratio E_{b}/N_0 in Fig. 9 (right). The update schedule parameter θ is defined according to (8), where $P_{\text{b,old}}(j)$ and $P_{\text{b,new}}(j)$ are the bit error probabilities. Again, the dashed curves correspond to $\theta = 0$, while the solid curves correspond to $\theta = 10^{-2}$, and the hollow circles indicate the $\mathcal{C}(3, 6, 15)$ ensemble, while the solid circles indicate the

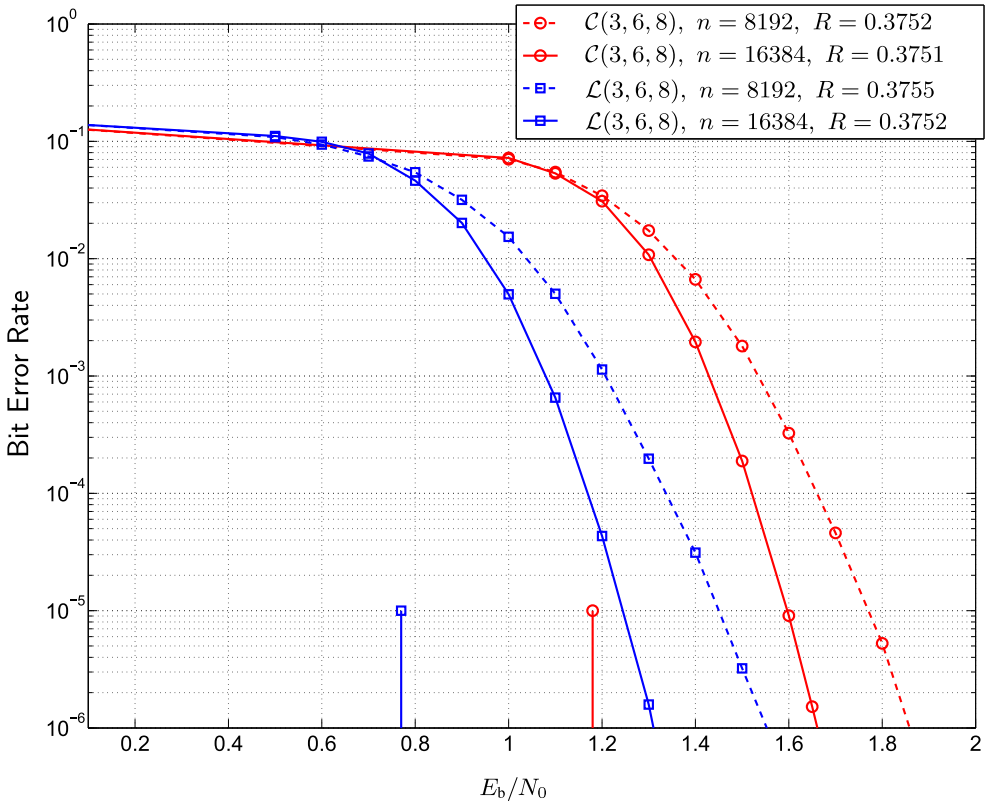

Fig. 10. Bit error rates on the AWGN channel for codes chosen from the $\mathcal{L}(3,6,8)$ ensembles with $M=256$ (dashed curve with squares) and $M=512$ (solid curve with squares) as well as for codes chosen from the $\mathcal{C}(3,6,8)$ ensembles with $M=512$ (dashed curve with circles) and $M=1024$ (solid curve with circles).

$\mathcal{L}(3,6,15)$ ensemble. The vertical straight lines show the corresponding thresholds. We again observe that the loop ensemble demonstrates a significant complexity improvement.

While $\bar{I}_{\text{eff}}$ is a convenient ensemble-based complexity measure, in order to compare the decoding complexity of finite-size codes, both the number of protograph nodes and the lifting factor M must be taken into account. Since the loop ensemble has $6L+4$ protograph nodes, i.e., twice as many as the corresponding single chain ensemble, a fair comparison involves selecting a lifting factor half as large, i.e., $M/2$, for the loop. The same scaling is applied in the simulation results presented in the next section. The full complexity then scales as $\bar{I}_{\text{eff}}M(3L+2)$ per iteration, where $\bar{I}_{\text{eff}}$ is computed as a function of the channel parameter separately for each ensemble.

F. Simulation Results

In the previous sections we have observed that connected chain ensembles have superior asymptotic decoding performance when compared to corresponding single chain ensembles. In this section we show that the connected chain structure also translates into improved decoding performance for finite code lengths by examining the finite length performance of connected chain ensembles used for transmission over the AWGN channel.

We consider two codes, one of length $n=8192$ and the other of length $n=16384$, randomly selected from the single chain ensemble $\mathcal{C}(3,6,8)$ with lifting factors $M=512$ and $M=1024$, respectively. In addition we randomly pick two codes from the loop $\mathcal{L}(3,6,8)$ ensemble, one with lifting factor $M=256$ and the other with $M=512$. The corresponding code lengths are also $n=8192$ and $n=16384$, respectively. The only condition imposed on the Tanner graphs of the selected codes was the absence of cycles of length four. The rate of all codes approximately equals $R=0.375$. The BERs for transmission over the AWGN channel are plotted in Fig. 10 as functions of E_b/N_0. The solid curves correspond to the BERs for the codes of length 16384 from the loop (solid curve with squares) and the single chain (solid curve with circles) ensembles, respectively. The BERs for the codes of length 8192 are given by the dashed curve with squares (loop ensemble) and the dashed curve with circles (single chain ensemble). The asymptotic iterative decoding thresholds for $\mathcal{C}(3,6,8)$ and $\mathcal{L}(3,6,8)$ ensembles are shown by the solid bars and equal to 1.19dB and 0.78dB respectively. The thresholds are computed from the values σ^* given in Table II and represented in terms of E_b/N_0. The simulated curves were obtained with 100 decoding iterations.

We note that the loop ensemble codes show better decoding performance and deliver a gain of approximately 0.4 dB with respect to the single chain ensemble codes. This happens despite the fact that the loop codes have smaller lifting factors M. Similar behavior has been demonstrated in [6], where the loop and single chain ensemble codes were compared for

TABLE IV
MINIMUM DISTANCE GROWTH RATES FOR SEVERAL LOOP AND SINGLE CHAIN ENSEMBLES

L	Rate	$\delta_{\min}$, $\mathcal{L}(3,6,L)$	$\delta_{\min}$, $\mathcal{C}(3,6,L)$
3	0.1667	0.2033	0.1419
4	0.2500	0.1313	0.0825
5	0.3000	0.0897	0.0570
6	0.3333	0.0354	0.0449
9	0.3889	0.0160	0.0287
10	0.4000	0.0136	0.0258
12	0.4167	0.0109	0.0214
15	0.4333	0.0085	0.0171
18	0.4444	0.0071	0.0142

transmission over the BEC, and the bit erasure rate curves were derived using an analytical approximation.

G. Minimum Distance Analysis

We define the *asymptotic spectral shape* of a linear code ensemble as

$$r(\delta) = \limsup_{n\to\infty} r_n(\delta), \tag{9}$$

where $r_n(\delta) = \frac{1}{n}\ln(A_{\lfloor \delta n \rfloor})$, $\delta = d/n$ is the normalized Hamming distance d, $n \in \mathbb{N}$ is the block length, and A_d is the ensemble weight enumerator. Suppose that the first positive zero crossing of $r(\delta)$ occurs at $\delta = \delta_{\min}$. If $r(\delta)$ is negative in the range $0 < \delta < \delta_{\min}$, then $\delta_{\min}$ is called the *minimum distance growth rate* of the code ensemble. By considering the probability

$$\Pr(d < n\delta_{\min}) \leq \sum_{d=1}^{\lfloor n\delta_{\min}\rfloor - 1} A_d = \sum_{d=1}^{\lfloor n\delta_{\min}\rfloor - 1} e^{nr_n(d/n)},$$

one can show (see references below) that, as the block length n becomes sufficiently large, $\Pr(d < n\delta_{\min}) \ll 1$, since $r_n(\delta) < 0$ for $\delta \leq \delta_{\min}$. Then we can say that with high probability a code, randomly chosen from the ensemble, has a minimum distance that is at least as large as $n\delta_{\min}$, *i.e.*, the minimum distance increases linearly with block length n. We refer to such an ensemble of codes as *asymptotically good*.

A technique to calculate the asymptotic spectral shape $r(\delta)$ for protograph-based block LDPC code ensembles was presented in [23], [24], and it was shown in [25]–[27] that ensembles of protograph-based (J, K)-regular single chain ensembles are asymptotically good. In this section we present the results of a similar protograph-based analysis for connected chain ensembles and demonstrate that they share the good distance properties of the individual chains.

The asymptotic minimum distance growth rates computed for the ensembles $\mathcal{L}(3, 6, L)$ are given in Table IV. We observe that, like the individual chain ensembles, the $\mathcal{L}(3, 6, L)$ ensembles are asymptotically good. As the length of the two chains forming the loop increases, the rate of the ensemble increases, the iterative decoding thresholds approach the optimum maximum a posteriori probability (MAP) decoding thresholds, and the minimum distance growth rate decreases. This is analogous to the effect of increasing the length L for the single chain ensemble $\mathcal{C}(3, 6, L)$ [18].

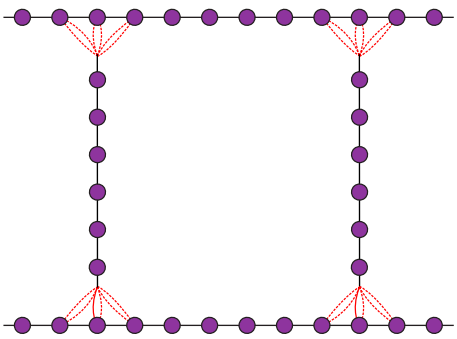

Fig. 11. Two single chain protographs of length $L = 12$ connected by two bridges of length $L_b = 6$ (a square ensemble).

We note that connecting two single chain protographs as proposed in this paper can only increase the number of edges at the variable nodes. It is known that any protograph where all the variable nodes are of degree three or larger corresponds to an asymptotically good ensemble [24]. Hence, connecting single-chain ensembles with variable nodes of degree three or higher guarantees that the connected ensemble is also asymptotically good. We notice that for $L < 6$ the loop ensembles have superior minimum distance growth coefficients compared to the single chains, since the connection points contribute significantly to the increase in the number of edges per variable node in the loop ensemble. For larger L, the growth coefficient of the loop is below that of the corresponding single chain, approaching approximately half of its value as L grows. This is expected, since for large L the connecting edges play a minor role from the minimum distance perspective and the loop acts like a collection of two single chains.

IV. DEGREES OF FREEDOM IN CONSTRUCTION

There are numerous degrees of freedom that can be used in constructing connected chain ensembles. In this section we present several promising ensembles designed by connecting single chain ensembles according to the chain interconnection principles discussed in Section III-D.

Connected chain ensembles can be constructed with a variety of connection geometries. For example, a *square ensemble* is constructed by connecting two longer parallel single chains of length L to two shorter chains of length $L/2$ called *bridges*. A graphical representation of a square ensemble with $L = 12$ is shown in Fig. 11. The four connection points, that have the same structure as those depicted in Fig. 2 (b), are located such that the inner part of the resulting protograph forms a square. It has been shown in [9] that, for both the BEC and AWGN channels, square ensembles outperform single chain ensembles of the same rate in terms of both threshold and decoding complexity.

The improvements resulting from chain interconnection also extend to codes with higher node degrees. To illustrate this point, we consider two types of loop ensembles constructed from $(4, 8)$-regular chains, one with the connection point depicted in Fig. 12 (a) and the other with the connection point shown in Fig. 12 (b). The first type of connection point is designed to keep the check node degree constant,

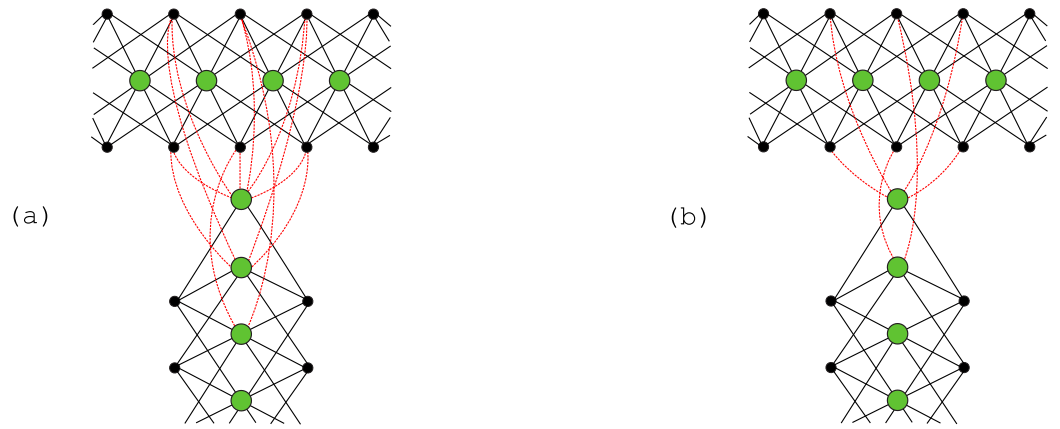

Fig. 12. Two ways of connecting $(4, 8)$-regular protograph chains. The connecting edges are shown with dashed lines.

TABLE V
BEC THRESHOLDS ϵ^* FOR THE LOOP ENSEMBLE $\mathcal{L}(3, 9, L)$ AND THE SINGLE CHAIN ENSEMBLE $\mathcal{C}(3, 9, L)$

L	R	$\mathcal{L}(3,9,L)$	$\mathcal{C}(3,9,L)$
6	0.5556	0.3746	0.3605
8	0.5883	0.3604	0.3392
12	0.6111	0.3437	0.3235
100	0.6600	0.3191	0.3196

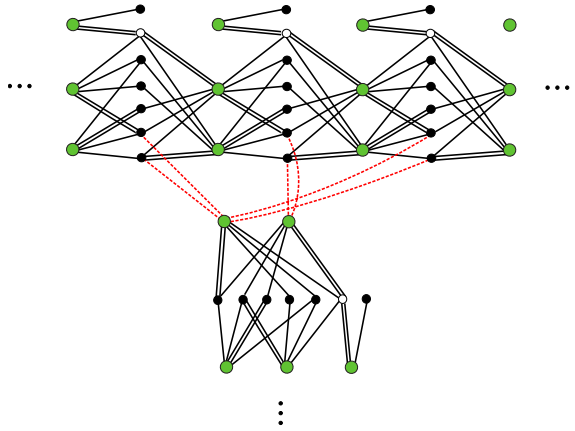

Fig. 13. Example connection point of two single chain AR4JA ensembles.

TABLE VI
BEC THRESHOLDS ϵ^* FOR SEVERAL SINGLE CHAIN ENSEMBLES $\mathcal{C}_{\text{AR4JA}}(L)$ AND LOOP ENSEMBLES $\mathcal{L}_{\text{AR4JA}}(L)$

Rate	Ensemble	ϵ^*	Ensemble	ϵ^*
0.611	$\mathcal{L}_{\text{AR4JA}}(6)$	0.3477	$\mathcal{C}_{\text{AR4JA}}(6)$	0.3388
0.633	$\mathcal{L}_{\text{AR4JA}}(10)$	0.3377	$\mathcal{C}_{\text{AR4JA}}(10)$	0.3331
0.638	$\mathcal{L}_{\text{AR4JA}}(12)$	0.3351	$\mathcal{C}_{\text{AR4JA}}(12)$	0.3330
0.644	$\mathcal{L}_{\text{AR4JA}}(15)$	0.3332	$\mathcal{C}_{\text{AR4JA}}(15)$	0.3330

TABLE VII
BEC THRESHOLDS ϵ^* FOR SEVERAL SINGLE CHAIN ENSEMBLES $\mathcal{C}_{\text{ARJA}}(L)$ AND LOOP ENSEMBLES $\mathcal{L}_{\text{ARJA}}(L)$

Rate	Ensemble	ϵ^*	Ensemble	ϵ^*
0.4167	$\mathcal{L}_{\text{ARJA}}(6)$	0.5189	$\mathcal{C}_{\text{ARJA}}(6)$	0.5159
0.4286	$\mathcal{L}_{\text{ARJA}}(7)$	0.5188	$\mathcal{C}_{\text{ARJA}}(7)$	0.5083
0.4444	$\mathcal{L}_{\text{ARJA}}(9)$	0.5060	$\mathcal{C}_{\text{ARJA}}(9)$	0.5015
0.4583	$\mathcal{L}_{\text{ARJA}}(12)$	0.5014	$\mathcal{C}_{\text{ARJA}}(12)$	0.4997
0.4667	$\mathcal{L}_{\text{ARJA}}(15)$	0.5001	$\mathcal{C}_{\text{ARJA}}(15)$	0.4996

while the second type, which is the same as for the $(3, 6)$ code chain in Fig. 2, has some reduced check node degrees. The geometry of the loop is the same as for the $\mathcal{L}(3, 6, L)$ ensemble, in the sense that the connection point splits a chain of length L into a short chain of length $\lfloor L/3 \rfloor$ and a long chain of length $\lfloor 2L/3 \rfloor$. Both loop ensembles outperform their corresponding single chain ensemble in terms of thresholds and decoding complexity, as shown in [8], while the loop with the second type of connection point exhibits the best threshold.

Connected chain ensembles with improved properties can also be constructed from codes with base rates other than $1/2$. For example, Table V compares the BEC thresholds ϵ^* of the loop ensemble $\mathcal{L}(3, 9, L)$ and the single chain ensemble $\mathcal{C}(3, 9, L)$ and demonstrates improved thresholds for the loop. Different types of chains can also be mixed in a connected construction, as presented in [7], where a loop consisting of a $(3, 6)$ chain and a $(4, 8)$ chain was shown to have a BEC threshold better than the individual thresholds of both connected single chains.

Chain interconnection can improve the properties of more advanced connected chain ensembles as well. Fig. 13 shows an example of a connection point for constructing a loop ensemble from two single chain AR4JA ensembles [24] that were shown to perform close to the BEC capacity limit [18]. Considering loops with the same geometry as for the $\mathcal{L}(3, 6, L)$ ensemble, Table VI lists the BEC thresholds ϵ^* of the single chain AR4JA ensembles $\mathcal{C}_{\text{AR4JA}}(L)$ with $L = 6, 10, 12$, and 15 (see [18]) along with the thresholds of the loop ensembles $\mathcal{L}_{\text{AR4JA}}(L)$ constructed by connecting two single $\mathcal{C}_{\text{AR4JA}}(L)$ chains. Again we note the improved thresholds of the loop ensembles. The same trend is observed when connecting single ARJA chains, as shown in Table VII, where the thresholds of the single chain $\mathcal{C}_{\text{ARJA}}(L)$ and loop $\mathcal{L}_{\text{ARJA}}(L)$ ensembles are compared.

Finally, we note that the improvement in decoding convergence of connected chain ensembles that manifests itself

both in terms of improved thresholds and reduced decoding complexity also translates to improved finite-length decoding error probability performance, as discussed in [6]. Further, we note that the connection of single chains can be done in a continuous fashion, thereby forming an infinite convolutional-like ensemble, as described in [15].

V. Conclusions

The connection of spatially coupled protograph chains provides an approach to extending the spatial graph coupling phenomenon from simple (single chain) graph coupling to more general coupled structures. We have presented several new types of protograph-based spatially coupled code ensembles formed by connecting single spatially coupled chains. These ensembles exhibit improved thresholds and reduced iterative decoding complexity. Input/output transfer functions of the components of a connected chain ensemble were shown to provide an indication of the limits of the decoding convergence of the connected chain ensemble, thus allowing their use as a tool to build more advanced structures.

Simulation results demonstrate that the asymptotic threshold and complexity improvements translate into improved finite-length performance. Moreover, we showed that the connected chain ensembles are asymptotically good in terms of minimum distance. Finally, we note that the principle of coupled chain connection is very general and may give rise to many other novel spatially coupled code ensemble constructions.

References

[1] A. J. Felström and K. S. Zigangirov, "Time-varying periodic convolutional codes with low-density parity-check matrix," *IEEE Trans. Inf. Theory*, vol. 45, no. 6, pp. 2181–2191, Sep. 1999.

[2] M. Lentmaier, A. Sridharan, D. J. Costello, Jr., and K. Sh. Zigangirov, "Iterative decoding threshold analysis for LDPC convolutional codes," *IEEE Trans. Inf. Theory*, vol. 56, no. 10, pp. 5274–5289, Oct. 2010.

[3] S. Kudekar, T. J. Richardson, and R. L. Urbanke, "Threshold saturation via spatial coupling: Why convolutional LDPC ensembles perform so well over the BEC," *IEEE Trans. Inf. Theory*, vol. 57, no. 2, pp. 803–834, Feb. 2011.

[4] S. Kudekar, T. J. Richardson, and R. L. Urbanke, "Spatially coupled ensembles universally achieve capacity under belief propagation," *IEEE Trans. Inf. Theory*, vol. 59, no. 12, pp. 7761–7813, Dec. 2013.

[5] S. Kumar, A. J. Young, N. Maoris, and H. D. Pfister, "A proof of threshold saturation for spatially-coupled LDPC codes on BMS channels," in *Proc. 50th Annu. Allerton Conf. Commun., Control, Comput.*, Monticello, IL, USA, Oct. 2012, pp. 176–184.

[6] P. M. Olmos, D. G. M. Mitchell, D. Truhachev, and D. J. Costello, Jr., "A finite length performance analysis of LDPC codes constructed by connecting spatially coupled chains," in *Proc. IEEE Inf. Theory Workshop*, Sevilla, Spain, Sep. 2013, pp. 1–5.

[7] D. Truhachev, D. G. M. Mitchell, M. Lentmaier, and D. J. Costello, Jr., "New codes on graphs constructed by connecting spatially coupled chains," in *Proc. Inf. Theory Appl. Workshop*, San Diego, CA, USA, Feb. 2012, pp. 392–397.

[8] D. Truhachev, D. G. M. Mitchell, M. Lentmaier, and D. J. Costello, Jr., "Improving spatially coupled LDPC codes by connecting chains," in *Proc. IEEE Int. Symp. Inf. Theory*, Boston, MA, USA, Jul. 2012, pp. 468–472.

[9] D. Truhachev, D. G. M. Mitchell, M. Lentmaier, and D. J. Costello, Jr., "Connecting spatially coupled LDPC code chains," in *Proc. IEEE Int. Conf. Commun.*, Ottawa, ON, Canada, Jun. 2012, pp. 2176–2180.

[10] R. Ohashi, K. Kasai, and K. Takeuchi, "Multi-dimensional spatially-coupled codes," in *Proc. IEEE Int. Symp. Inf. Theory*, Istanbul, Turkey, Jul. 2013, pp. 2448–2452.

[11] Y. Liu, Y. Li, and Y. Chi, "Spatially coupled LDPC codes constructed by parallelly connecting multiple chains," *IEEE Commun. Lett.*, vol. 19, no. 9, pp. 1472–1475, Sep. 2015.

[12] H. Kwak, B. Jun, P. Yang, J.-S. No, and D.-J. Shin. (2016). "New coupled codes constructed by overlapping circular SC-LDPC codes." [Online]. Available: https://arxiv.org/abs/1602.01577

[13] R. Tanaka and K. Ishibashi, "Robust coded cooperation based on multi-dimensional spatially-coupled repeat-accumulate codes," in *Proc. IEEE Wireless Commun. Netw. Conf.*, San Francisco, CA, USA, Mar. 2017, pp. 1–6.

[14] L. Schmalen and K. Mahdaviani, "Laterally connected spatially coupled code chains for transmission over unstable parallel channels," in *Proc. 8th Int. Symp. Turbo Codes Iterative Inf. Process.*, Bremen, Germany, Aug. 2014, pp. 77–81.

[15] P. M. Olmos, D. G. M. Mitchell, D. Truhachev, and D. J. Costello, Jr., "Improving the finite-length performance of long SC-LDPC code chains by connecting consecutive chains," in *Proc. 8th Int. Symp. Turbo Codes Iterative Inf. Process.*, Bremen, Germany, Aug. 2014, pp. 72–76.

[16] P. M. Olmos, D. G. M. Mitchell, D. Truhachev, and D. J. Costello, Jr., "Continuous transmission of spatially coupled LDPC code chains," *IEEE Trans. Commun.*, vol. 65, no. 12, pp. 5097–5109, Dec. 2017.

[17] J. Thorpe, "Low-density parity-check (LDPC) codes constructed from protographs," Jet Propuls. Lab., Pasadena, CA, USA, INP Prog. Rep. 42-154, Aug. 2003.

[18] D. G. M. Mitchell, M. Lentmaier, and D. J. Costello, "Spatially coupled LDPC codes constructed from protographs," *IEEE Trans. Inf. Theory*, vol. 61, no. 9, pp. 4866–4889, Sep. 2015.

[19] M. Lentmaier, D. V. Truhachev, K. S. Zigangirov, and D. J. Costello, Jr., "An analysis of the block error probability performance of iterative decoding," *IEEE Trans. Inf. Theory*, vol. 51, no. 11, pp. 3834–3855, Nov. 2005.

[20] T. J. Richardson and R. Urbanke, *Modern Coding Theory*. Cambridge, U.K.: Cambridge Univ. Press, 2008.

[21] S.-Y. Chung, "On the construction of some capacity-approaching coding schemes," Ph.D. dissertation, Dept. Elect. Eng. Comput. Sci., Massachusetts Inst. Technol., Cambridge, MA, USA, Sep. 2000.

[22] M. Lentmaier, M. M. Prenda, and G. P. Fettweis, "Efficient message passing scheduling for terminated LDPC convolutional codes," in *Proc. IEEE Int. Symp. Inf. Theory*, St. Petersburg, Russia, Jul./Aug. 2011, pp. 1826–1830.

[23] A. Sridharan, M. Lentmaier, D. V. Truhachev, D. J. Costello, Jr., and K. S. Zigangirov, "On the minimum distance of low-density parity-check codes with parity-check matrices constructed from permutation matrices," *Problems Inf. Transmiss.*, vol. 41, no. 1, pp. 33–43, Jan./Mar. 2005.

[24] D. Divsalar, S. Dolinar, C. R. Jones, and K. Andrews, "Capacity-approaching protograph codes," *IEEE J. Sel. Areas Commun.*, vol. 27, no. 6, pp. 876–888, Aug. 2009.

[25] A. Sridharan, D. Truhachev, M. Lentmaier, D. J. Costello, and K. S. Zigangirov, "Distance bounds for an ensemble of LDPC convolutional codes," *IEEE Trans. Inf. Theory*, vol. 53, no. 12, pp. 4537–4555, Dec. 2007.

[26] D. Truhachev, K. S. Zigangirov, and D. J. Costello, Jr., "Distance bounds for periodically time-varying and tail-biting LDPC convolutional codes," *IEEE Trans. Inf. Theory*, vol. 56, no. 9, pp. 4301–4308, Sep. 2010.

[27] D. G. M. Mitchell, A. E. Pusane, and D. J. Costello, Jr., "Minimum distance and trapping set analysis of protograph-based LDPC convolutional codes," *IEEE Trans. Inf. Theory*, vol. 59, no. 1, pp. 254–281, Jan. 2013.

Dmitri Truhachev received the Ph.D. degree in electrical engineering from Lund University, Sweden. He is currently an Associate Professor in the Department of Electrical and Computer Engineering, Dalhousie University, Canada. Before joining Dalhousie University, he held postdoctoral and research associate positions at the University of Alberta, Canada. His research interests include error-correction codes, spatial graph coupling, multi-user communications, fiber optic communications, and underwater acoustic communications.

David G. M. Mitchell received the Ph.D. degree in electrical engineering from the University of Edinburgh, U.K., in 2009. From 2009 to 2015 he held Post-Doctoral Research Associate and Visiting Assistant Professor positions with the Department of Electrical Engineering, University of Notre Dame, USA. Since 2015, he has been an Assistant Professor with the Klipsch School of Electrical and Computer Engineering, New Mexico State University, USA. His research interests are in the area of digital communications, with emphasis on error control coding and information theory.

Michael Lentmaier is an Associate Professor at the Department of Electrical and Information Technology at Lund University, which he joined in January 2013. His research interests include design and analysis of coding systems, graph based iterative algorithms and Bayesian methods applied to decoding, detection and estimation in communication systems. He received the Dipl.-Ing. degree in electrical engineering from University of Ulm, Germany in 1998, and the Ph.D. degree in telecommunication theory from Lund University, Sweden in 2003. He then worked as a Post-Doctoral Research Associate at University of Notre Dame, Indiana and at University of Ulm. From 2005 to 2007 he was with the Institute of Communications and Navigation of the German Aerospace Center (DLR) in Oberpfaffenhofen, where he worked on signal processing techniques in satellite navigation receivers. From 2008 to 2012 he was a senior researcher and lecturer at the Vodafone Chair Mobile Communications Systems at TU Dresden, where he was heading the Algorithms and Coding research group. He is a senior member of the IEEE and served as an editor for IEEE COMMUNICATIONS LETTERS (2010-2013), IEEE TRANSACTIONS ON COMMUNICATIONS (2014–2017), and IEEE TRANSACTIONS ON INFORMATION THEORY (since April 2017). He was awarded the Communications Society and Information Theory Society Joint Paper Award (2012) for his paper "Iterative Decoding Threshold Analysis for LDPC Convolutional Codes".

Daniel J. Costello, Jr. received the B.S.E.E. degree from Seattle University, Seattle, WA, in 1964, and the M.S. and Ph.D. degrees in Electrical Engineering from the University of Notre Dame, Notre Dame, IN, in 1966 and 1969, respectively. Dr. Costello joined the faculty of the Illinois Institute of Technology, Chicago, IL, in 1969. In 1985 he became Professor of Electrical Engineering at the University of Notre Dame, and from 1989 to 1998 served as Chair of the Department of Electrical Engineering. In 1999, he received a Humboldt Research Prize from the Alexander von Humboldt Foundation in Germany. In 2000, he was named the Leonard Bettex Professor of Electrical Engineering at Notre Dame, and in 2009 he became Bettex Professor Emeritus.

Dr. Costello has been a member of IEEE since 1969 and was elected Fellow in 1985. He served 18 years as a member of the Information Theory Society Board of Governors, and in 1986 he was President of the BOG. In 2000, the IT Society selected him as a recipient of a Third-Millennium Medal. In 2009, he was co-recipient of the Donald G. Fink Prize Paper Award, which recognizes an outstanding survey, review, or tutorial paper in any IEEE publication issued during the previous calendar year. In 2012, he was a co-recipient of the joint IT Society/COM Society Prize Paper Award, which recognizes an outstanding research paper in the IT or COM Transactions during the previous two calendar years. In 2013, he received the Aaron D. Wyner Distinguished Service Award from the IT Society, which recognizes outstanding leadership in and long standing exceptional service to the IT community. In 2015 he received the IEEE Leon K. Kirchmayer Graduate Teaching Award, which recognizes inspirational teaching of graduate students in the IEEE fields of interest.

Dr. Costello's research interests are in digital communications, with special emphasis on error control coding and information theory. He has more than 400 technical publications in his field, and in 1983 he co-authored a textbook entitled "*Error Control Coding: Fundamentals and Application*", the 2nd edition of which was published in 2004.

Alireza Karami received the B.A.Sc. degree in electrical engineering from University of Tabriz, Iran in 2006, and the M.A.Sc. degree in communications from Khajeh Nasir University of Technology, Tehran, Iran in 2009. He is currently pursuing his Ph.D. degree in the area of telecommunications at Dalhousie University, Canada. His research interests include error correction coding, spatial graph coupling, and multi-user communications.